Paper presented at the COMPENG-2018 conference, Oct. 10-12 2018, Florence, Italia

Highly stable rotating machine models using the state-space-nodal real-time solver

Christian Dufour
Opal-RT Technologies
Montréal, Québec, Canada
christian.dufour@opal-rt.com

***Abstract*—This paper presents a set of rotating machine models, namely synchronous, asynchronous and permanent magnet synchronous machines, with increased stability characteristics compared to traditional state-space based methods. In this work, the machine models are all derived using the state-space-nodal (SSN) theory. This results in machine models that are stable without any parasitic load or numerical snubber. This is an important improvement for these models in solver packages based on the state-space approach, such as SimPowerSystems or PLECS.**

***Index Terms*—Hardware-In-the-Loop simulation, State-Space-Nodal, SSN, SimPowerSystems, Synchronous machine, induction machine, PMSM.**

I. Introduction

Real-time simulation is an important part of power system and industrial drive development as it enables engineers to test system controllers in the lab before field commissioning. The availability of accurate rotating machine models is also important in this regard.

A lot of work has been done over the years to achieve real-time capable rotating machine models. A good explanation of synchronous machine (SM) modeling theory is provided in [4]. In [5], various SM models, so-called dq0, VBR, PM, PM-dq0 are discussed and compared extensively.

Permanent magnet synchronous machine (PMSM) models are simpler than SM typically, because they involve less windings. This relative simplicity makes it possible to run PMSM drive models on FPGA chips, together with full non-linear inductances profile in the phase domain [6].

As for induction motor (IM) models, including doubly-fed types, many models exists in the literature; the most common again makes use of Park's transform [4]. They can also be implemented on FPGA.

In this paper, we derive SM, IM and PMSM models directly from their state-space equations using the SSN methodology. This results in a systematic way of deriving rotating machinery models compatible with simulation software based on the nodal admittance approach. These models turn out to be more robust and stable than the one using the current injection with delay method, commonly used in state-space simulation packages such as PLECS and SPS.

II. State-Space-Nodal (SSN) theory

The State-Space-Nodal solver [1] is a nodal admittance solver in which the branch discrete companion model (DCM) equations are directly derived from their state-space equations.

Suppose there is a group of resistance, inductance, capacitance, switches and transformer sources, and other electrical elements (i.e. a generalized branch or SSN group) connected to a terminal of unknown voltage and current (a 'nodal connection point'). The state-space equation usually exists:

$$\begin{aligned} x' &= A_k x + B_k u \\ y &= C_k x + D_k u \end{aligned} \tag{1}$$

where

x: states of the system
u: inputs of the system
y: output of the system

A_k , B_k , C_k , D_k : state space matrices corresponding to the k-th permutation of switches and other piecewise linear element segments.

When discretized, these equations result in:

$$x_{n+1} = A_d x_n + B_{d1} u_n + [B_{d2(in)} \quad B_{d2(no)}] \begin{bmatrix} u_{n+1(in)} \\ u_{n+1(no)} \end{bmatrix}$$

$$\begin{bmatrix} y_{n+1(in)} \\ y_{n+1(no)} \end{bmatrix} = \begin{bmatrix} C_{(in)} \\ C_{(no)} \end{bmatrix} x_{n+1} + \begin{bmatrix} D_{(in,in)} & D_{(in,no)} \\ D_{(no,in)} & D_{(no,no)} \end{bmatrix} \begin{bmatrix} u_{n+1(in)} \\ u_{n+1(no)} \end{bmatrix} \tag{2}$$

where:

A_d,B_{d1}, B_{d2}, C , D are the discrete state matrices for the present pattern of binary switches modeled inside the group (switch pattern index k is not shown);

$u_{(in)}$: internal sources of the state-space model. Like in standard state-space modeling, these include known forced sources and sources from non-linear current injections.

$u_{(no)}$: unknown sources of the state-space model at the present time n+1. This represents the nodal voltages or the current injection that can only be resolved by simultaneous solution of all groups connected to the nodes of the network.

$y_{(in)}$: internal outputs of the model. These are usually current and voltage measurements to be taken inside the group;

$y_{(no)}$: nodal outputs of the state-space model. These are the voltage or current outputs of the group that need to be solved simultaneously along with all other groups of the system.

The trapezoidal rule of integration will produce $B_{d1} = B_{d2}$ while most other discretization methods will produce different discrete B_d matrices. Backward-Euler method for example produces a null B_{d1} matrix. Subscript *n* and *n+1* indicate the time instants separated by the discretization time step.

Equation 2 can be written in the following way:

$$y_{n+1(no)} = C_{(no)}\{A_d x_n + B_{d1} u_n + B_{d2(in)} u_{n+1(in)} + \dots \\ B_{d2(no)} u_{n+1(no)}\} + D_{(no,in)} u_{n+1(in)} + D_{(no,no)} u_{n+1(no)} \quad (3)$$

which can be grouped into implicit and explicit terms. The explicit part refers to known values at the current time step in Eq. 3, including internal source values at instant *n+1*. This is a 'history term' in EMTP jargon.

$$y_{hist} = C_{(no)}\{A_d x_n + B_{d1} u_n + \dots \\ B_{d2} u_{n+1(in)}\} + D_{(no,in)} u_{n+1(in)} \quad (4)$$

The other terms compose the implicit part, which contains the terms in *n+1* linked to nodal quantities, not solvable a priori from the equation alone. With voltage components in inputs *u* and current components in the corresponding outputs *y*, the implicit relation

$$W = C_{(no)} B_{d2(no)} + D_{(no.no)} \quad (5)$$

has an admittance unit if $u_{n+1(no)}$ is a voltage source, which is the case for machines models, and corresponds to the 'discrete admittance' term in EMTP jargon, therefore resulting in a Norton-type DCM. SSN also allows to derive Thevenin-type DCM if the nodal inputs are currents and outputs are voltages in Eq. 2. In that case W represent an impedance.

The various sets of SSN-derived DCM are then assembled to form a nodal admittance problem, which solution is used to complete the implicit part of DCM equations at each time step.

III. SSN FOR ROTATING MACHINES

Rotating machines such as synchronous machine, asynchronous machine and permanent magnet machine can be described with state-space equations and therefore can be derived from and included in the SSN solution. Because of the inductive nature of common rotating machines, they will result in Norton-type DCM with voltage sources as inputs.

A. Synchronous machine

The SSN model of the Synchronous machine (SM) is similar to the one from SimPowerSystems (SPS) and EMTP-RV: the electrical part is represented by a fifth-order (salient rotor) or sixth-order (round rotor) state-space model. The model takes into account the dynamics of the stator, field, and up to 3 damper windings. The equivalent circuit of the model is represented in the rotor reference frame (dq0 frame). All rotor parameters and electrical quantities are viewed from the stator. The quote sign (') refers to rotor quantities.

The following Park transformation used to express all quantities in the reference frame attached to rotor, where θ is the rotor angle, is given by:

$$T = S.\sqrt{\tfrac{2}{3}}.\begin{bmatrix} 1 & -1/2 & -1/2 \\ 0 & \sqrt{3}/2 & -\sqrt{3}/2 \end{bmatrix} \quad (6a)$$

where

$$S = \begin{bmatrix} \cos(\theta) & \sin(\theta) \\ -\sin(\theta) & \cos(\theta) \end{bmatrix} \quad (6b)$$

The machine equations are then equal to (^ indicates time derivative):

$$\widehat{\psi} = (-RL^{-1} + \Omega)\psi + \begin{bmatrix} V_{dqf} \\ \mathbf{0}_3 \end{bmatrix} \quad (7a)$$

$$I_{dqf} = L^{-1}_{(first\ 3\ row)}\psi \quad (7b)$$

with $V_{dqf} = [V_{sd}\ V_{sq}\ V_f\ ]^t$, $\psi = [\psi_{sd}\ \psi_{sq}\ \psi'_f\ \psi'_{kd}\ \psi'_{kq1}\psi'_{kq2}]^t$, $I_{dqf} = [I_{sd}\ I_{sq}\ I'_f\ ]^t$, $R = diag(R_s, R_s, R'_f, R'_{kd}, R'_{kq1}, R'_{kq2})$
Indices *kd*, *kq1* and *kq2* correspond to dampers along d and q.

$$\Omega = \begin{bmatrix} 0 & \omega_e & 0 & 0 & 0 & 0 \\ -\omega_e & 0 & 0 & 0 & 0 & 0 \\ 0 & 0 & 0 & 0 & 0 & 0 \\ 0 & 0 & 0 & 0 & 0 & 0 \\ 0 & 0 & 0 & 0 & 0 & 0 \\ 0 & 0 & 0 & 0 & 0 & 0 \end{bmatrix}$$

$$L = \begin{bmatrix} L_d & 0 & L_{md} & L_{md} & 0 & 0 \\ 0 & L_q & 0 & 0 & L_{mq} & L_{mq} \\ L_{md} & 0 & L'_f & L_{md} & 0 & 0 \\ L_{md} & 0 & L_{md} & L'_{kd} & 0 & 0 \\ 0 & L_{mq} & 0 & 0 & L'_{kq1} & L_{mq} \\ 0 & L_{mq} & 0 & 0 & L_{mq} & L'_{kq2} \end{bmatrix}$$

In the inductance matrix L_{md} represents the d-axis mutual inductance and L_d, L'_f, L'_{kd} are the sum of each winding leakage and mutual inductance (same for q-axis). ω_e is the electric pulsation frequency in rad/s. Ω is often called the 'speed term'.
Using the following Park transform,

$$V_{dqf} = \begin{bmatrix} T & \mathbf{0_2} \\ \mathbf{0}_3^t & ns/nf \end{bmatrix} V_{abcf} \quad I_{abcf} = \begin{bmatrix} T^t & \mathbf{0}_3 \\ \mathbf{0}_2^t & ns/nf \end{bmatrix} I_{dqf} \quad (8)$$

where V_{abcf} is the vector of machine terminal voltage to ground (including the field terminal) and I_{abcf} is the vector of current entering the terminals.

The SSN equations of the synchronous machine are found by combining Eq. 8 with Eq. 7, thus obtaining the phase domain state-space equations of the SM. Discretizing with trapezoidal rule of integration results in an equation in the form Eq. 2, from which the Norton-type SSN DCM is derived from Eq. 4 and 5.

In Eq.8, the ns/nf term is the stator coil to field coil turn ratio; this term is required to obtain the proper SSN admittance from the physical field coil terminals. With the nominal field current known i_{fn}, one can obtain this turn ratio by using the following formula:

$$ns/nf = L_{md} i_{fn} \omega_{base} / V_{base} \quad (9)$$

where ω_{base} is the base electric frequency in rad/s and V_{base} is the nominal line-to-line RMS voltage of the machine.

The synchronous machine zero-sequence equations are treated similarly. The SSN equations for the zero-sequence are similar to d-q ones, except that:

$$\widehat{\psi} = (-R_0 L_0^{-1})\psi + T_0 V_{abcn} \quad (10a)$$
$$I_{abcn} = T'_0 L_0^{-1} \psi \quad (10b)$$

with $T_0 = \sqrt{\frac{1}{3}}.[1\ 1\ 1 - 3]$. R_0 is equal to the stator resistance, R_s while L_0 is equal to the stator leakage inductance $L_{ls} = L_d - L_{md}$. The V_{abcn} vector includes the neutral to ground voltage. Electric torque is given by:

$$T_e = pp.(\psi_d i_q - \psi_q i_d) \quad (11)$$

where *pp* denotes the number of poles pairs. .

B. Asynchronous machine or induction machine

An induction machine (IM) model with fixed d-q (Park) referential can be used to obtain the SSN equations. The Park transformation used to express all quantities in the reference frame attached to the stator is given as in eq. 6 with $\theta = 0$ for stator quantities and $\theta = -\theta_{rotor}$ for rotor quantities. It leads to the following relations

$$V_{dqs} = T.V_{abcs} \qquad I_{abcs} = T^t.I_{dqs} \quad (12a)$$
$$V'_{dqr} = {}^{ns}/_{nr}\, T.V_{abcr} \qquad I'_{abcr} = {}^{ns}/_{nr}\, T^t.I_{dqr} \quad (12b)$$

The stator to rotor turn ratio ${}^{ns}/_{nr}$ is required in Eq. 12b to pass the rotor voltages and currents to and from the stator point of view. Additionally, indices s and r correspond to stator and rotor entities, respectively, with primed rotor variables being referred to the stator). The machine equations are then equal to:

$$\widehat{\psi} = (-RL^{-1} + \Omega)\psi + V_{dq} \quad (13a)$$
$$I_{dq} = L^{-1}\psi \quad (13b)$$

with $V_{dq} = [V_{sd}\ V_{sq}\ V'_{rd}\ V'_{rq}]^t$, $\psi = [\psi_{sd}\ \psi_{sq}\ \psi'_{rd}\ \psi'_{rq}]^t$,

$$R = diag(R_s, R_s, R'_r, R'_r), \quad \Omega = \begin{bmatrix} 0 & 0 & 0 & 0 \\ 0 & 0 & 0 & 0 \\ 0 & 0 & 0 & -\omega_e \\ 0 & 0 & \omega_e & 0 \end{bmatrix}$$

where ω_e is the electric frequency of the rotor given by: $\omega_e = pp.\omega_m$ and ω_m is the rotor speed in rad/s. Also note that $L_s = L_m + L_{sl}$ (similarly for rotor), where L_{sl} is the stator leakage inductance.

$$L^{-1} = \frac{1}{L'_r L_s - L_m^2} \begin{bmatrix} L'_r & 0 & -L_m & 0 \\ 0 & L'_r & 0 & -L_m \\ -L_m & 0 & L_s & 0 \\ 0 & -L_m & 0 & L_s \end{bmatrix}$$

with $R_s, L_s, R'_r, L'_r, L_m$ being the stator resistance and inductance, the rotor resistance and inductance referred to the stator and mutual inductance. Electric torque is equal to:

$$T_e = pp.(\psi_{ds} i_{qs} - \psi_{qs} i_{ds}), \quad (14)$$

with the absence of scaling factor due to the use of orthonormal Park transformations.

The SSN discrete companion model equations are obtained from the phase-domain equations of the IM, obtained again by combining Eq. 12 and 13, resulting in a time-variant phase-domain model for the IM with V_{abc} as input and I_{abc} as outputs. (Variant because of matrix S for the rotor, speed terms and saturation effects in matrix *L*). Once discretized, it produces a discrete equation in the form of Eq 3, from which the DCM is obtained readily by Equations 4 and 5. During the SSN solution, terms 4 and 5 are included in the nodal admittance solution. Because the DCM is time-variant, it requires SSN to re-factorize the nodal admittance matrix at each time step.

C. Permanent magnet synchronous machine (PMSM).

The SSN PMSM model is derived from the classic d-q model using Park transformation, but this time with $\theta = \theta_{rotor}$, i.e. the reference frame is attached to the rotor, yielding:

$$\widehat{\psi} = (-RL^{-1} + \Omega)\psi - \omega_e \Psi + TV_{abc} \quad (15a)$$
$$I_{abc} = T^t L^{-1} \psi \quad (15b)$$

with $= [\psi_{sd}\ \psi_{sq}]^t$, $R = diag(R_s, R_s)$, $L = \begin{bmatrix} L_d & 0 \\ 0 & L_q \end{bmatrix}$,

$\Omega = \begin{bmatrix} 0 & \omega_e \\ -\omega_e & 0 \end{bmatrix}$ and $\Psi = \begin{bmatrix} 0 \\ \sqrt{\frac{3}{2}}\lambda \end{bmatrix}$ (back-EMF term on the q-axis with the peak magnet flux λ being on the d-axis), *pp* the number of pair of poles and ω_e the electric pulsation frequency in rad/s.

Electric torque is computed with the following formula

$$T_e = pp.\{\sqrt{\frac{3}{2}}\lambda\omega_e i_q + (L_d - L_q) i_d i_q\} \quad (16)$$

IV. Analysis of the Instability of Delayed injection method used in several software packages

The so-called 'delayed-current injection method' (DCIM) is a commonly used simulation method for complex devices such as rotating machines. SimPowerSystems and PLECS notably use this method which is prone to numerical instability. DCIM for machine models uses the same machine equations described in the previous section, describing the machines as a state-space system with voltage inputs and current outputs. But, as the name say, DCIM alternatively compute the network machine terminal

voltages, then computes the machine currents and uses these currents as injections to the next network solution, etc... A delay therefore exists between the network and the machine solutions and this delay is the main source of instability of this approach.

In this section, we propose to explain mathematically the source of this instability using Bode frequency analysis. Instinctively, we know that connecting a current source to an inductive or high impedance circuit is looking for trouble. In real-life, this often triggers arcs. In simulation, instability results.

Bode frequency analysis can be useful to understand the problem at stake. The method has been used already to study Power Hardware-In-the-Loop (PHIL) stability [14] or multi-rate stability[16]. Alternately, z-domain stability analysis using Routh criteria can also be done for PHIL[13].

Fig. 1 shows a simple grid-connected inductor simulated as a delayed current injection and the corresponding closed-loop diagram. Two closed loop diagrams are presented, one with a ideal integrator with delay, and one with a Forward Euler integrator.

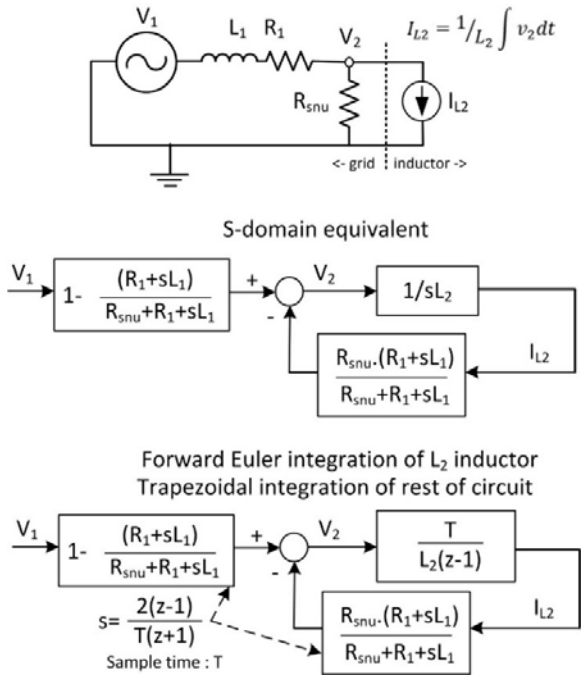

Fig. 1 Numerical stability test circuit and equivalent control diagrams (T is sample time)

For the purpose of this test, we set the grid inductance (L_1) equal to the delayed inductance (L_2, mimicking a machine inductance for example), both equal to 0.1 mH. We also set the grid resistance (R_2) to have a quality factor of 20. The Bode analysis is made for snubber resistance (R_{snu}) values of 6,8,10 and 12 Ω with a sample time of 20 µs and depicted in Fig. 2 The figure shows that case with 6 and 8 Ω have a positive gain margin at 180 degrees phase shift. The case with 10 Ω has no gain margin and is marginally stable. Finally, the case with 12 is unstable because the open loop gain is greater than 1 at 180 degree of phase shift. These stability findings are fully supported by actual simulation of the case.

Interestingly enough, changing the snubber from a resistance to a series RC snubber do not change the stability property of the circuit. This can be viewed in Fig. 3 where a 1 µF was added to the snubber of the previous case: it does not change the gain margin at 180 degrees phase shift. The usage of R-C snubber is however useful to obtain a higher impedance and lower power losses induced by the snubber at the main network frequency.

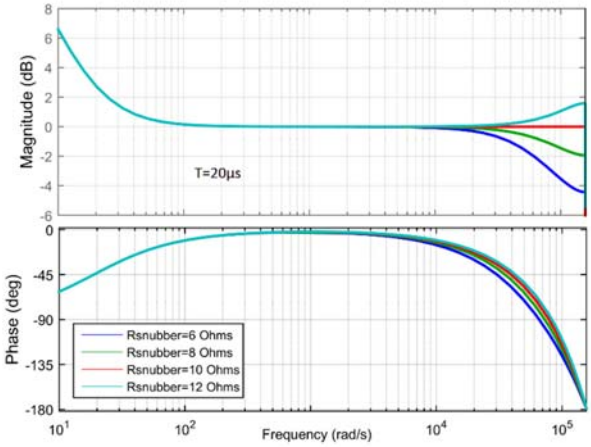

Fig. 2 Bode analysis of Forward Euler inductance coupled with trapezoidal integration of rest of network, case with simple R snubber

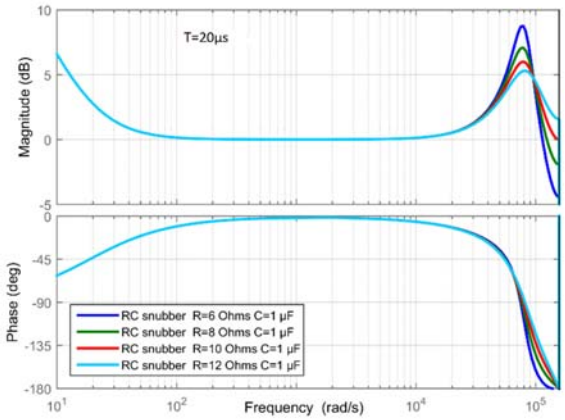

Fig. 3 Bode analysis of Forward Euler inductance coupled with trapezoidal integration of rest of network, case with R-C snubber

Integration by trapezoidal rule of both inductor L_2 and the rest of the circuit produces a maximum phase shift of 90 degrees in Bode analysis (resistive snubber case) and is always stable therefore (result not shown). The problem of computing the model remains however because of the loop without delay induced by trapezoidal integration of both branches. This problem can be solved either by combining both branches before discretization or the use of an implicit solver method like nodal admittance method such as SSN.

V. EXAMPLE CASES

In this section, we will highlight the accuracy of the SSN-derived machine model and in particular, their great numerical stability when connected to negligible loads or inductive-type elements, such as transformers, without any use of numerical snubbers.

For each machine model type (SM, IM and PMSM), we will now describe such a case.

A. Synchronous machine with field rectifier test case

In this test case, we compare the SSN solver with the classic SPS at a very small simulation time step using a real-life model of an SM with a field current rectifier, depicted in Fig. 4 The SM is connected to a main grid through a transformer and the field thyristor rectifier is also fed with a second transformer. In the test, we bring the SM terminal voltage to 1 pu by closed-loop control of the field current thyristor rectifier while driving the SM to 0.8 pu of the nominal power (202 MVA) through the closed-loop action of SM turbine and governor. Saturation was not considered in this test.

From this stable operation point, the following actions are then made:

- At 11 sec. (on the graphs), a single-phase fault to ground is made;
- 0.095 sec. after the fault, the field coil is short-circuited by the non-linear discharge resistance (Fig. 5);
- 0.1 sec. after the fault, the SM stator breaker is opened and the field rectifier is opened;
- 0.15 sec. after the fault, the fault is cleared.

Fig. 6 Fig. 7 show the results; an excellent match is obtained between SPS 1µs and SSN 25µs.

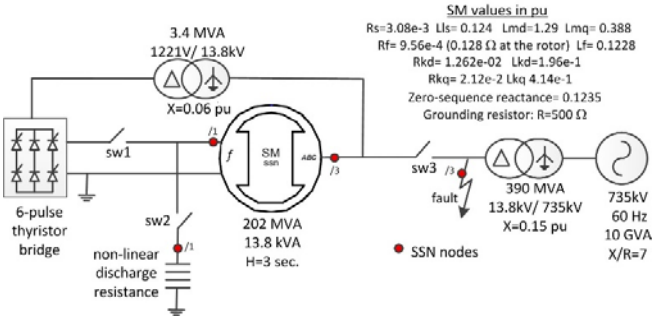

Fig. 4 Synchronous machine with field rectifier case

1) Numerical stability comparison

One main difference between the SSN and SPS simulations is that the former does NOT require any parasitic load at the MS terminal. By comparison, SPS requires a parasitic load of 5 MW (2.5% of nominal power) at 25 µs and even 200 kW at 1 µs. In the present test, made at 0.8pu of the rated machine power, the effect of this parasitic load is not critical but it may become important in cases where the SM is driven at lower power levels.

The reason for this parasitic load requirement for SPS is the current injection with delay used, as well as other state-space-based simulation software such as PLECS.

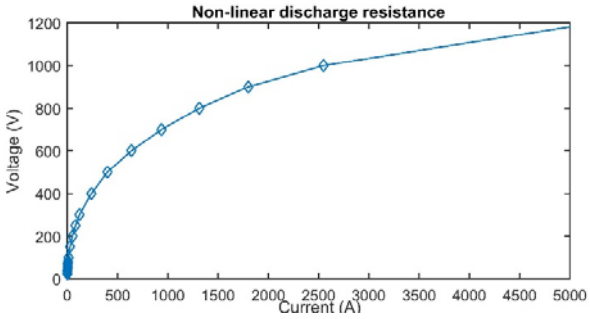

Fig. 5 Non-linear discharge resistance characteristic

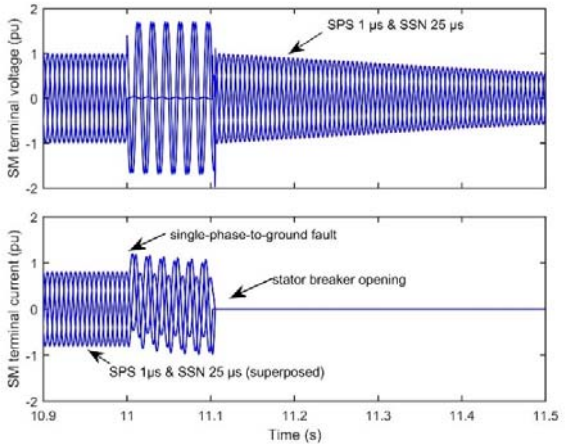

Fig. 6 SM voltages and currents

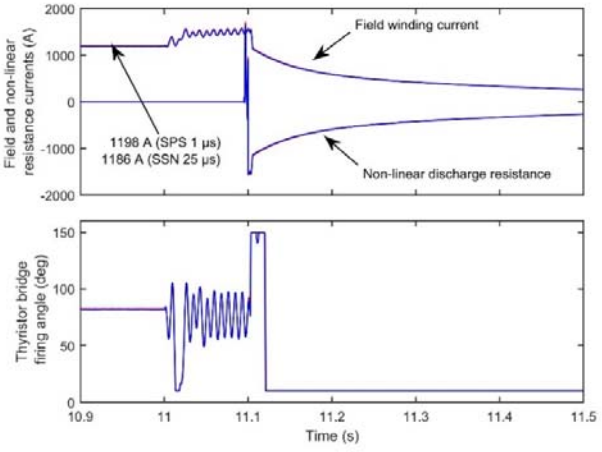

Fig. 7 Field and non-linear discharge resistance currents (upper) Thyristor bridge firing angle (lower)

2) Non-linear resistance iterations in real-time

The real-time test model contains a non-linear resistance that was modeled using the MOV iterative model described in [3].

B. Two asynchronous machines test case

In this test, we compare the SSN asynchronous machine models, in squirrel-cage (IM) and wound-rotor doubly-fed (DFIM) configurations, against the standard SPS models. The test circuit is described in Fig. 8 along with major parameters. Both machines run at constant speed with 2% slip. At 0.9 seconds, the DFIM rotor resistance is short-circuited; this is followed by a 3-phase-to-ground fault at the network at 1 second, which is cleared at 1.2 sec. Finally, the DFIM is disconnected from the grid by sw2 at 1.3 sec. Results for the DFIM and IM currents are given in Fig. 9 and 10 respectively. In these figures, we see that currents are well-superposed between the SSN simulation at 25 µs and the SPS one at 1µs.

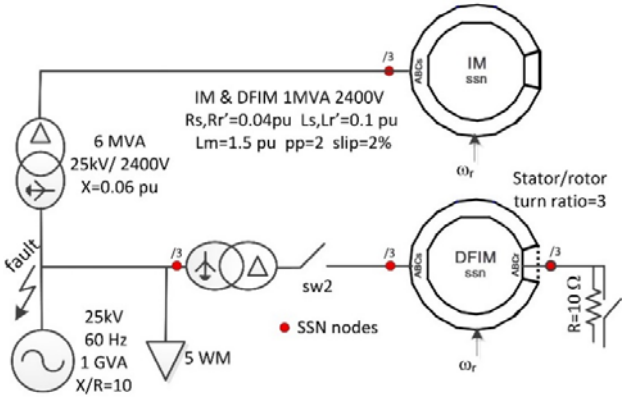

Fig. 8 Test case with 2 asynchronous machines

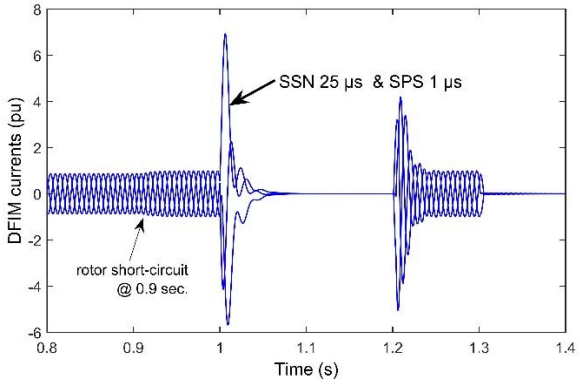

Fig. 9 DFIM currents

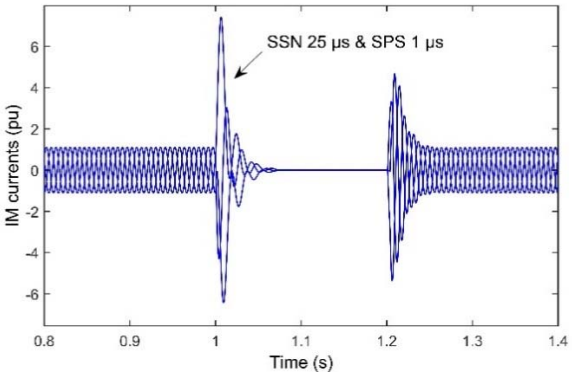

Fig. 10 Squirrel-cage induction machine currents.

1) Numerical stability comparison

In the case just presented, it was found that a minimum load of 50kW (5% of the DFIM rating) was required to maintain the stability of the DFIM when **sw2** opens (Fig. 8 using SPS at 25 µs. In the SSN case, no load was required at all. Even at 1 µs, a small load of 2 kW was required to maintain the SPS stability (and included in the presented results).

The reason for this parasitic load requirement for SPS is again the current injection with delay used in it, as well as other state-space-based package such as PLECS.

C. PMSM drive vector control test case

This test case is about the PMSM SSN model, which we compare with SPS at a very small simulation time step, taken as a reference.

A most common usage of PMSM is combined with an IGBT inverter. We present here a case that was already studied in [2], in which two problems had to be addressed:

- A relatively high PWM frequency with regards to the simulation time step, possibly leading to inaccuracies in active drive mode.
- A stability problem when the inverter is left in so-called 'free-running' mode, that is when the inverter gating are not pulsing, and also in case one phase of the motor is opened, due to a fault one IGBT leg, for example.

In [2], this problem was addressed relatively well, using interpolated switching function methods that handle high-frequency PWM very well but were still suffering from stability issues. Maximum high-impedance values were typically under 1000 Ohms in this case.

The model, depicted in Fig. 11 used in this test consists of a diode rectifier feeding a DC-link from which a PMSM IGBT 2-level drive is controlled using a PWM vector controller. The PMSM and the vector controller are the exact same one as in [2] with the exception of PWM frequency, which was raised from 2.25 to 9 kHz.

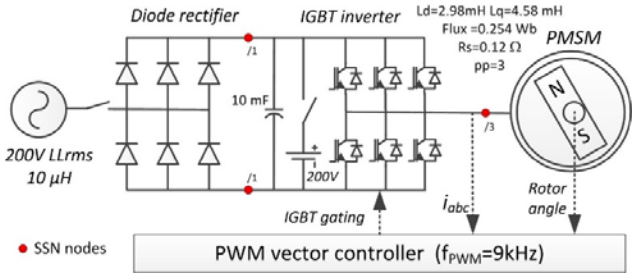

Fig. 11 PMSM drive test case

The test performs the following actions:

- PMSM acceleration to 1000 rpm at 0.05 sec.
- At 0.15 sec, phase A is opened
- From 0.2 to 0.4 sec, the motor is accelerated to 2000 rpm (with the open phase)
- At 0.4, the DC-link voltage is forced to 200V.
- At 0.45, IGBT gates are turned OFF, resulting in the natural rectification by the IGBT bridge and deceleration of the PMSM.

Results, depicted in Fig. 12 almost prefectly match between the SSN case at 10 µs and the SPS case at 1 µs.

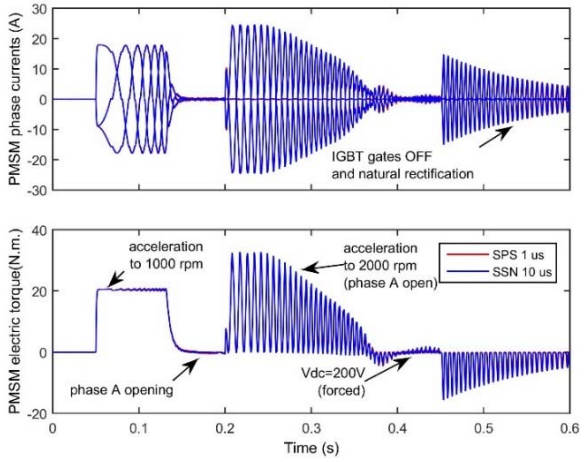

Fig. 12 PMSM currents and torque

1) Numerical stability comparison

In the open-phase mode of the test, the maximum resistance of the open fault in SPS is under 1000 Ohms at 10 µs. Over this value, the model becomes unstable (by the virtue of the current injection technique of SPS). In the SSN case by comparison, this open fault resistance can be well over 100000 Ohms, resulting in improved accuracy in this mode. It is also worth to note that the 9 kHz PWM disqualify the use of SPS at 10 µs for accuracy reasons. This technique is somehow similar the Time-Stamped-Bridge (TSB) used by Mitsubishi Electric in [2]. The difference is that TSBs are interpolated switching functions, while SSN interpolation occurs within the state-space equations directly.

2) Numerical accuracy comparison

A current injection with delay method (CIDM) is used in SPS and PLECS. CIDM can be used because the internal PMSM equation are solved with Forward Euler method (or Trapezoidal plus one delay), an explicit method. This enables the main state-space solver and the CIDM model of the PMS to 'alternate' their solutions, computing one after the other.

By contrast, SSN is an implicit solver. This means that the solution for the PMSM equations are made simultaneously with the main state-space equation of the rest of the network.

We are showing next a small test case where some differences can be observed between the 2 approaches. The test consists of driving the same PMSM drive with a constant 200V DC, a rotor speed of 200 rad/s and letting phase A of the inverter in 'high' position while phase B and C are in 'lower' position (in other words: phase A of the PMSM is at 200V and phases B-C are grounded).

The results of the test are depicted in Fig. 13 They show that the motor current runs quite high, above 1000A. Closer examination shows that the SPS simulation at 10 µs is a little bit less accurate than SSN at 10 µs and SPS at 1 µs, the latter considered as a reference. Further tests (not shown) demonstrated that SSN have a precision similar to SPS when the speed term is included with a delay in the SSN equations. The speed term of the PMSM is included with a delay in SPS (as of release 2017a); more explanations are given about this topic in Section VII-A about SSN LDL^T factorization.

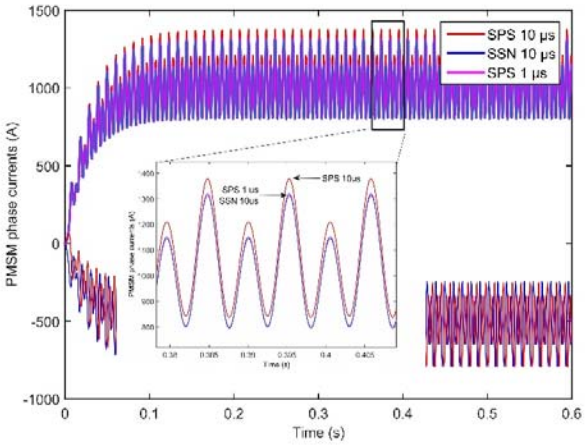

Fig. 13 Fixed-voltage PMSM test

D. More-Electric Aircraft variable-frequency starter-generator

More-Electric Aircraft (MEA) is a relatively new paradigm in aircraft design in which power electronic is used more extensively than ever in subsystems. Boeing 787 Dreamliner is a good example of MEA.

The VFSG model, described in Fig. 14 is comprised of three 3-phase machines, all mounted on a common shaft: a permanent

magnet generator (PMG), a synchronous machine exciter (i.e. a synchronous machine with rotating stator) and a main synchronous generator. The exciter machine output is always connected to the main machine field via a rotating rectifier. During generator operation, the PMG supplies AC voltage to the excitation system, regulated using a power electronics converter feeding the field winding of the exciter SM. In start mode, before the VFSG is rotating, an external voltage source (battery storage system, for instance) replaces the PMG.

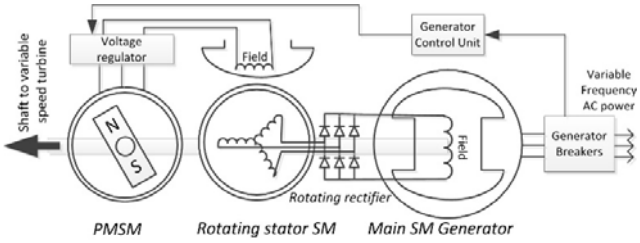

Fig. 14 MEA VFSG configuration

The test sequence consists in the starting of the variable-frequency starter generator unit (VFSG). The VFSG allows the plane's engines to reach the required speed for ignition. During the start sequence, the voltage regulator applies a high frequency sinusoidal voltage at the field windings of the exciter machine. The field created by this voltage induces a voltage in the coils connected to the rotating rectifier unit, which ultimately provides the excitation for the main machine. Using a 10 kHz inverter along with field-oriented control (FOC), the engine shaft is accelerated. HIL was achieved by loopback on the simulator using Digital In/Out.

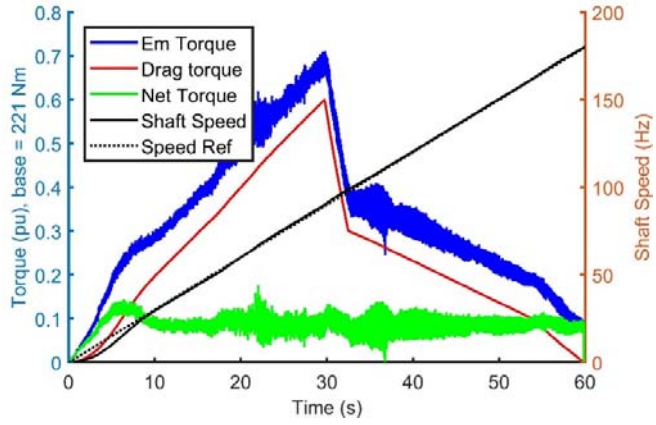

Fig. 15 VFSG start sequence: torques and speeds

As seen on Fig. 15 the drag torque increases until t=30s, when the engine starts providing torque to the shaft. After t=60s, the engine has fully ignited and sets the speed of the shaft; the VFSG switched to generation mode. The voltage regulator stops injecting the high frequency voltage and uses the voltage provided by the stator of the Pilot Exciter. The VFSG is now in self-excitation mode, using permanent magnet generator.

1) Solver requirements for high-speed VFSG

In Fig. 15 the main synchronous machine, having 2 pairs of poles, is brought to an equivalent electric speed of 400 Hz. In steady-state, the VSFG runs in the 400-800Hz range. At such speeds, it has been found that the synchronous machine model cannot use a delayed-speed term in its equations for accurate and stable simulations. This in turn forbids the use of LDL^T solver; LU solver must be used MEA applications. See Section VIII-A for more details.

One consequence of this is that neither LDL^T nor Cholesky-based nodal solvers can be used in theses MEA applications because of the symmetric nodal matrix assumption.

VI. SSN MACHINE MODEL PROGRAMMABILITY

These SSN machine models are particular cases of SSN User Custom Block (SSN-UCB), which allows users to incorporate their own electric modules into the SSN nodal admittance solver. We show here how this is done for the PMSM.

1) SSN DCM determination for the PMSM

Detailed SSN DCM derivation is made here. The same method is used for other machines. For the PMSM we have the continuous time matrices

$$A = (-RL^{-1} + \Omega) \quad B_{(in)} = \sqrt{\frac{3}{2}}\lambda \quad B_{(no)} = \mathrm{T}$$
$$C = T'L^{-1} \quad \mathrm{D} = 0, \tag{17}$$

with $u_{(in)} = \omega_e$, $u_{(no)} = V_{abc}$ and $y_{(no)} = I_{abc}$.

Discretization with trapezoidal rule with a time-step *h* gives:

$$A_d = \left(I - \frac{Ah}{2}\right)^{-1}\left(I + \frac{Ah}{2}\right) B_{d1} = B_{d2} = \frac{Bh/2}{I - Ah/2} \quad \text{(with } B = [B_{(in)}\ B_{(no)}]\text{) and } C_d = C$$

The DCM admittance is then equal to $Y_{dcm} = C_d B_{d2(no)}$ and the DCM history source is equal to:

$$I_{hist} = C_{\mathrm{d}}\{A_d\psi_n + B_{d1}u_{n(in)} + B_{d1}u_{n(\,no)} + B_{d2}u_{n+1(in)}\}$$

2) DCM calculation using Simulink blocks

While SSN-UCB can be coded as Simulink S-functions, in the present work however, the machine UCB's were coded using *only* Simulink blocks. This is a major advantage in terms of programmability of the SSN solver over methods that requires C-like coding of Simulink S-functions.

VII. Real-time performance

All the models presented in this paper run in real-time on the *eMEGAsim* Digital Real-Time Simulator (DRTS).

TABLE I: REAL-TIME PERFORMANCE ON X10-XEON

Model	Model calculation time (µs)	SSN nodes
SM	8.5	8
IM +DFIM	6.7	12
PMSM	5.7	5
VFSG	9.5	8

Table I shows the calculation time step of the complete models described by Fig. 4 including controls, on a single core of the DRTS running under RT-Lab 11 and using Xeon X10 processors. 20 cores are available in the standard DTRS as of 2016. Standard LU factorization was used.

The SSN machine models developed in this paper are all in the category of so-called 'variable admittance' model. This means that their DCM equation varies at each time step. Therefore LU factorization must be done at each time step for the nodes where these SSN machines are connected and this increases the computational time.

In contrast, CIDM models (of SPS and PLECS) don't have this issue because they don't contribute at all to the admittance matrix. This advantage comes with decreased numerical stability as we demonstrated in this paper.

VIII. Further model enhancements

It is possible enhance the presented model in terms of performance and features.

A. LDL^T factorization and machine models

Recent versions of SSN offer the possibility to use an LDL^T factorization of the SSN nodal admittance matrix, instead of the traditional LU one. LDL^T factorization is close to twice as fast as LU in theory but requires the admittance matrix to be symmetric. Unfortunately, the incorporation of the speed term Ω in the A matrix cause the admittance matrix of the machines to be asymmetrical. The solution to this problem is to move Ω to the input part of the state-space equations, with a delay on the flux vector. For the PMSM for example, this gives:

$$\dot{\psi} = -RL^{-1}\psi + \Omega\psi_{del} - \omega_e\Psi + TV_{abc}$$

where ψ_{del} is the delayed state vector, taken as input now.

Delayed speed term is used in the EMTP Theory book [4] and the dq0 model described in [5]. It is less precise that direct incorporation in the state matrix A but can lead to faster models because A is symmetric. Precision is improved by using a one-step prediction on delayed flux vector.

B. Iron losses and saturation

In some applications, such as in electric vehicle drives where volume is critical, PMSMs are usually designed with maximum torque per volume, high power density and possibly non-negligible machine core losses due to eddy currents and hysteresis. In [10], the classic d-q axis PMSM model was augmented with a shunt resistance in both axes to represent the core losses. This approach can be applied to SSN-based motor models.

Advanced saturation capabilities could therefore be implemented in the models. For example, leakage flux saturation [11] could be implemented in the synchronous machine.

IX. Discussion

This paper's objective was to demonstrate that the SSN theory can be used to develop rotating machine models in a systematic and generalized way and also that the resulting models were more stable than current-injection with delay method (CIDM) used in most state-space simulation packages such as SPS and PLECS today.

The theory and equations of SM, IM/DFIM and PMSM are well known in the literature. This paper showed that all these models could be translated *methodically* into discrete-time models usable in *any* nodal admittance based simulation package. The word *any* is important and really means that after the models are determined, they can be used in any nodal admittance based package, such as EMTP or the HYPERSIM real-time simulator.

The second aspect of the paper is about the numerical stability of the SSN models. The paper demonstrated that the resulting models could be used without parasitic load or RC-snubber at the terminal of the machines in cases where the machine gets suddenly connected to high-impedance or opened-circuits. This stability property is mainly due to the simultaneity of the machine and grid solutions in nodal admittance based solvers such as SSN.

By comparison, CIDM alternates between machine and grid solutions. This delayed solution method is a major source of instability when the machines are connected to inductive circuits. Another way to view this is that they are less accurate with low loads because they require a minimal artificial load to remain stable. This requirement of CIDM models for parasitic loads or snubbers was also demonstrated using Bode method in the paper.

In high-speed applications interestingly, it was found that delayed-speed terms methods were inaccurate and forced the use of the LU solver of SSN because of the asymmetry of the admittance matrix. Therefore LDL^T or Cholesky factorization cannot be used for MEA applications.

The SSN models shown in this paper are available in the ARTEMiS plug-in for SimPowerSystems [12] software package.

X. APPENDIX 1: SATURATION IN SYNCHRONOUS MACHINES

Saturation is considered in the SSN-SM model using the total air-gap flux magnitude $\psi_{mag} = \sqrt{\psi_{md}^2 + \psi_{mq}^2}$, which is the flux that passes only through the mutual inductances. The simplest and common way to consider saturation is to modify L_{md} and L_{mq} dynamically during simulation according to the equivalent linear inductance at the operating point.

However this is not accurate in transient conditions because only the steady-state magnetization inductance is considered then. A more precise way to include saturation is to use the linearized inductance at the point of operation [4][5]. Fig. 16 shows the difference between the linear inductance L_{lin} and the incremental inductance L_{inc}. The latter as the effect of creating a flux offset ψ_0 which must be carefully considered. In this case, the SM equations are transformed to take the 'incremental fluxes' $\psi^{"}$ as state variables. We this change of variable we obtain:

$$\psi = \psi_0 + \psi^{"} \tag{18a}$$

$$\widehat{\psi}^{"} = (-RL_{inc}^{-1} + \Omega)\psi^{"} + \Omega\psi_0 - \frac{\mathrm{d}\psi_0}{\mathrm{dt}} + V_{daf} \tag{18b}$$

$$I_{daf} = L_{\mathrm{inc}}^{-1}\psi^{"} \tag{18c}$$

in which ψ_0 and L_{inc} are continuously updated according to the operating point. A unique saturation curve is used here and the following formulas are used to part into d- and q-axis values for round rotor machines:

$$L_{inc-d} = L_{inc} \ , \ L_{inc-q} = (L_{mq}/L_{md})L_{inc} \ ,$$
$$\psi_{0-d} = (\psi_{md}/\psi_{mag})\psi_0 \ , \ \psi_{0-q} = (\psi_{mq}/\psi_{mag})\psi_0 \tag{19}$$

With salient rotor machines, this is done only for d-axis.

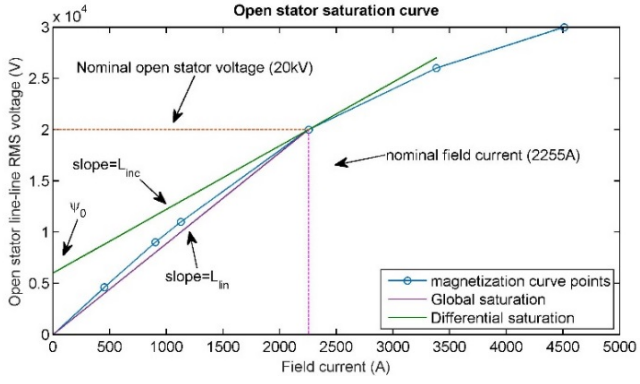

Fig. 16 Typical open stator synchronous machine saturation curve

REFERENCES

[1] C. Dufour, J. Mahseredjian , J. Bélanger, "A Combined State-Space Nodal Method for the Simulation of Power System Transients", IEEE Transactions on Power Delivery, Vol. 26, no. 2, April 2011 (ISSN 0885-8977), pp. 928-935

[2] M. Harakawa, C. Dufour, S. Nishimura, T.Nagano, "Real-Time Simulation of a PMSM Drive in Faulty Modes with Validation Against an Actual Drive System", Proceedings of the 13th European Conference on Power Electronics and Applications (EPE-2009), Barcelona, Spain, Sept. 8-10, 2009

[3] C. Dufour, O. Tremblay, "Iterative Algorithms of Surge Arrester for Real-Time Simulators", 18th Power Systems Computation Conference (PSCC'14), Wroclaw, Poland, August 18-22, 2014.

[4] H.W. Dommel, EMTP Theory Book, 2nd edition.

[5] U. Karaagac, J. Mahseredjian, and O. Saad, "An efficient synchronous machine model for electromagnetic transients," IEEE Trans. Power Del., vol. 26, no. 4, pp. 2456–2465, Oct. 2011

[6] C. Dufour, S. Cense, T. Yamada, R. Imamura, J. Bélanger, "FPGA Permanent Magnet Synchronous Motor Floating-Point Models with Variable-DQ and Spatial Harmonic Finite-Element Analysis Solvers", 15th Power Electronics and Motion Control Conference, EPE-PEMC 2012, Novi Sad, Serbia, Sept. 4-6, 2012

[7] G. J. Rogers, D. S. Benaragama, "An Induction Motor Model with Deep-Bar Effect and Leakage Inductance Saturation" Archiv fur Elektrotechnik, Vol. 60, pp. 193-201, 1978

[8] M. Sokola, E. Levi, A novel induction machine model and its application in the development of an advanced vector control scheme, International Journal of Electric Engineering Education, 37/3, July 2000, pp.233-248

[9] C. Dufour, S. Cense, T. Yamada, R. Imamura, J. Bélanger, "FPGA Permanent Magnet Synchronous Motor Floating-Point Models with Variable-DQ and Spatial Harmonic Finite-Element Analysis Solvers", 15th Power Electronics and Motion Control Conference, EPE-PEMC 2012, Novi Sad, Serbia, Sept. 4-6, 2012

[10] A. Zabihinejad, P. Viarouge , S. Roy , J. Cros, "Efficient Design of a High Speed PMSM Drive for Electric Vehicle Application Using Real Time Simulator", Journal of Asian Electric Vehicles, Volume 13, Number 2, December 2015

[11] J.C Flores, G.W. Buckley, G. McPherson, "The effect of saturation on the armature leakage reactance of large synchronous machines", IEEE Trans. Power App. Syst., Vol. PAS-103, pp. 593-600, March 1984

[12] ARTEMiS v7.2.2, OPAL-RT Technologies, www.opal-rt.com

[13] M. Hong, Y. Miura, T. Ise, Y. Sato, T. Momose and C. Dufour, "Stability and Accuracy Analysis of Power Hardware-in-the-loop Simulation of Inductor Coupled Systems", *IEEJ Trans. IA*, Vol. 130, No. 7, pp.902-912 (2010)

[14] M. O. Faruque et al. (IEEE PES Task Force on Real-Time Simulation of Power and Energy Systems), "Real-Time Simulation Technologies for Power Systems Design, Testing, and Analysis", IEEE Power and Energy Technology Systems Journal, June 2015é

[15] Kelu Xu, Ning Xie, Chengmin Wang and Xudong Shi, Modeling and Simulation of Variable Speed Variable Frequency Electrical Power System in More Electric Aircraft', The Open Electrical & Electronic Engineering Journal, 2017, 11, 87-98, DOI: 10.2174/1874129001711010087

[16] L. A. Grégoire, H. F. Blanchette, J. Bélanger and K. Al-Haddad, "Real-Time Simulation-Based Multisolver Decoupling Technique for Complex Power-Electronics Circuits," in *IEEE Transactions on Power Delivery*, vol. 31, no. 5, pp. 2313-2321, Oct. 2016.